Evaluating spiny mice (*Acomys*) as a model for cardiac research

Kazuhiro Shindo[1*], Hsuan Peng[1*], Renée R. Donahue[1], Brooke M. Ahern[2], Bryana M. Levitan[2], Jonathan Satin[2], Ashley W. Seifert[3], Ahmed Abdel-Latif[1,4]

[1] Saha Cardiovascular Research Center, College of Medicine, University of Kentucky
[2] Department of Physiology, College of Medicine, University of Kentucky
[3] Department of Biology, University of Kentucky
[4] Gill Heart and Vascular Institute and Division of Cardiovascular Medicine, University of Kentucky and the Lexington VA Medical Center

***Both authors contributed equally to the study.**

Abstract

Complex tissue regeneration is extremely rare among adult mammals. An exception, however, is the superior tissue healing of multiple organs in spiny mice (*Acomys*). While *Acomys* species exhibit the remarkable ability to heal complex tissue with minimal scarring, little is known about their cardiac structure and function. In this study, we characterized cardiac structure, anatomy, and *in vivo* function, as well as cardiomyocyte characteristics in *Acomys* compared to the most commonly used cardiac mouse model, the C57BL6 mouse strain (*Mus*). Our results demonstrate comparable cardiac anatomy, structure and function between the two rodent species, but reveal significant differences in their cardiomyocyte characteristics. These findings establish *Acomys* as a new mammalian model for cardiac research.

31 **Introduction**

32 Significant clinical advances in revascularization and medical therapies have
33 improved the mortality rate after myocardial infarction (MI).[1] Unfortunately, there are no
34 therapies to limit myocardial damage during MI and millions of patients progress to develop
35 heart failure (HF). This is because the normal healing response to tissue injury in adult
36 mammals is fibrotic repair; an effective short-term strategy, but one that leads to loss of tissue
37 function. Following injury to the heart, a limited ability to replace functional cardiomyocytes
38 results in irreversible damage, scar formation, and compromised heart function. These events
39 will ultimately lead to HF.[2] Although robust cardiac regeneration occurs in some adult
40 vertebrates (e.g., zebrafish, salamanders, newts, etc.) and neonate mammals,[3-6] adult
41 mammalian hearts exhibit poor regenerative capacity.[7-9] The lack of adult mammalian models
42 demonstrating cardiac regeneration has contributed to the current knowledge gap in the field.

43 The ability to regenerate injured organs is widespread in the animal kingdom. Fishes,
44 newts, and salamanders have extensive regenerative ability, and can functionally replace most
45 tissues and organs after amputation. Specifically, zebrafish have become a well-characterized
46 model for adult cardiac regeneration with the documented ability to recover from a plethora of
47 heart injuries including apical resection,[6] cryo-injury,[10] and coronary artery ligation. In contrast,
48 most adult mammals generally exhibit poor regenerative capacity, especially as it pertains to
49 recovering from heart damage. Spiny mice (*Acomys spp.*) are murid rodents found throughout
50 Africa, the Middle East and Western Asia. These rodents exhibit a number of special traits,[11]
51 tantamount among them is the ability to regenerate skin and complex tissue.[12-16] Moreover, a
52 recent study examining acute and chronic kidney injury documented enhanced cytoprotection
53 in *Acomys cahirinus* compared to two laboratory mouse strains.[17] At present, the extent to
54 which spiny mice respond to heart injury remains unknown. In order to characterize the heart
55 injury response in a comparative framework, it is imperative to accurately determine *Acomys*

heart structure and function. Here, we report detailed cardiac characterization of *A. cahirinus* in comparison to the commonly used C57BL6 mouse strain. The results of this study demonstrate comparable cardiac anatomy, structure and function between *Acomys* and *Mus* hearts but differences in cardiomyocyte phenotype between species.

Methods

Animal care

Male *Acomys cahirinus* (6-8 months old, in-house breeding colony) and *Mus musculus* (C57Bl6, 8-12 weeks old, Jackson Laboratory, Bar Harbor, ME) were housed at the University of Kentucky, Lexington, KY. *Acomys* were housed individually in metal wire cages (Quality Cage Company, Portland, OR) and fed a 3:1 mixture by volume of 14% protein mouse chow (Teklad Global 2014, Harlan Laboratories, Indianapolis, IN) and black-oil sunflower seeds (Pennington Seed Inc., Madison, GA).[11] All animal procedures were approved by the University of Kentucky Institutional Animal Care and Use Committee (IACUC #: 2019-3254 and 2011-0889).

Echocardiography

Echocardiography was acquired with a Vevo 3100 (VisualSonics, Toronto, Canada) equipped with a MX550D 25-55 MHz linear array transducer. Baseline cardiac function was assessed as previously described.[18] A heating pad and rectal temperature probe were utilized to keep body temperature at 37°C during the experiment. Modified parasternal long-axis and short-axis was utilized to determine left ventricular function and volume in M-mode, two-dimensional and Doppler echocardiography modes. We also used M-mode tracings at the mid-papillary level to estimate the systolic and diastolic parameters, and Teichholz formula at end-systole and end-diastole to measure the left ventricle (LV) volumes. All mice were

81 anaesthetized using 1%–3% isoflurane during Echocardiography to maintain a heart rate of
82 450–500 BPM for all echocardiographic acquisitions. Echocardiographic imaging and analysis
83 were performed by a blinded investigator.
84
85 **Coronary anatomy**
86 Mice received an i.p. injection of heparin (100 units in 300ul sterile PBS) to prevent
87 coagulation. Ten minutes later, mice were injected with TRITC-Dextran according to the
88 method of Hoffmann et al (2011). Briefly, mice were anesthetized and 0.5ml of TRITC-Dextran
89 (Sigma # 42874, 40 kDa, 100mg/ml) was injected via retro-orbital route and the animal
90 returned to anesthesia. After two minutes, mice were euthanized via cervical dislocation and
91 the heart excised for imaging using the Maestro EX *in vivo* Imaging System (Cambridge
92 Research & Instrumentation Inc., USA) using a blue filter (λex 500 nm; λem 750 nm long in
93 10-nm steps). Images were imported into Nikon AR (Version 4.51.01) for cropping and scale
94 bar representation.
95 In a separate cohort, mice received an i.p. injection of heparin (100 units in 300ul
96 sterile PBS) to prevent coagulation. Ten minutes later, under isoflurane anesthesia, hearts were
97 excised and cannulated with a blunt tip 23g needle and clamp. 10 ml of 1x PBS was perfused
98 intra-aortically, followed by 1.5ml Batson's 17 polymer mixture (2.5ml base monomer + 600ul
99 Catalyst + 3 drops Promoter; Polysciences). Polymer was mixed and ten minutes later was
100 injected over five minutes and then left to cure on ice for 3 hours. Once cured, hearts were
101 briefly washed with ddH2O and then placed in potassium hydroxide (maceration solution) for
102 one hour at room temp. After maceration incubation, hearts were laid with the anterior side up
103 and the left anterior descending artery was imaged using a Nikon Camera (DS-12) after
104 application of several drops of ddH2O to clear overlying tissue.
105

106 **Tissue collection and Histology**

107 Tissue from all species were collected and weighed immediately at sacrifice. The dry
108 lung weight was collected after 3 days of 65° C incubation. Hearts were perfused with PBS
109 (VWR International) followed by 4% buffered formalin (VWR International) fixation via
110 cannulation of the ascending aorta. Hearts were post-fixed overnight at 4^0 C. Hearts were then
111 sectioned into 3-mm cross-sectional slices followed by paraffin embedding. Tissue was
112 transferred to 70% ethanol until sectioning into 4-µm sections starting at the level of papillary
113 muscle.

114

115 **Immunofluorescence**

116 Immunohistochemical assessments were carried out on deparaffinized and rehydrated
117 sections as previously described.[18] After deparaffinization, washing, TRIS heat induced epitope
118 retrieval, and protein and streptavidin/biotin blocking, slides were incubated with primary
119 antibody: Isolectin B4 (L-2140, Sigma, St. Louis, MO) overnight at 4°C. After washing,
120 sections were incubated with secondary antibody conjugated to streptavidin-Alexa Fluor 568
121 (S11226, Thermo Fisher Scientific, Waltham, MA) for 30 minutes, and cover slipped with
122 mounting medium containing DAPI counterstain (Vector #H-1200). 10–20 adjacent areas per
123 section were examined at 40x magnification using Nikon A1 Confocal Microscope in the
124 University of Kentucky Confocal Microscopy facility. Data were presented as total capillary
125 density per mm^2.

126 **Cardiomyocyte isolation**

127 Ventricular cardiomyocytes were isolated as previously described.[19] Briefly, mice
128 received an i.p. injection of heparin (0.3ml of 1000 units/ml) prior to sacrifice. Mice were then
129 anesthetized with 1 -3 % Isoflurane. Hearts were excised and immediately perfused on a
130 Langendorff apparatus with a high-potassium Tyrode buffer and then digested with 5 to 7 mg

131 of liberase (Roche Applied Science). After digestion, atria were removed, and ventricular
132 myocytes were mechanically dispersed. Some isolated ventricular cardiomyocytes were used
133 for measuring cell surface area and nuclei, and the others were used for electrophysiological
134 recordings and calcium transients. Calcium concentrations were gradually restored to
135 physiological levels in a stepwise fashion for electrophysiological studies, and only healthy
136 quiescent ventricular myocytes were used for electrophysiological analysis within 12 h.
137

138 **Cell surface area, t-tubule quantification, and nuclear number**

139 Isolated ventricular cardiomyocytes were incubated with primary antibodies:
140 Troponin T (MA512960, Thermo Fisher Scientific, Waltham, MA). After washing,
141 cardiomyocytes were incubated with secondary antibody conjugated to Alexa Fluor 594
142 (ab175700, Abcam, Cambridge, MA) and Hoechst (H3570, Thermo Fisher Scientific, Waltham,
143 MA) nuclear counterstain. 100 cardiomyocytes per animal were examined using Nikon
144 ECLIPSE E600 Microscope. For t-tubule quantification, live ventricular cardiomyocytes were
145 stained with Di-8-ANNEPES for 30 min to stain the cell membrane. AutoTT was used to
146 measure t-tubule density[20].
147

148 **Ploidy measurement**

149 Cardiomyocyte ploidy analyses were done with modification.[21] Isolated ventricular
150 cardiomyocytes were enriched by centrifugation at 3000 RPM for 1 minute and resuspended
151 in PBS supplemented with 1% goat serum. DAPI was added to the cell suspension (1:10,000
152 dilution) 3 mins prior to FACS. Cardiomyocyte sorting was performed on a cell sorter system
153 (iCyt-Sony) at room temperature. Nucleation was gated on height and width of signal from a
154 380 nm laser. Spleen cells from each species were also collected and sorted as diploid control.
155

156 **Electrophysiological recordings and calcium transients**

157 $I_{Ca,L}$ was recorded in the whole-cell configuration of the patch clamp technique as
158 previously described.[19] All recordings were performed at room temperature (20 to 22 °C). The
159 pipette solution consisted of (in mmol/liter) 125 Cs-methanosulfonate, 15 TEA-Cl, 1 MgCl2,
160 10 EGTA, and 5 Hepes, 5 MgATP, 5 phosphocreatine, pH 7.2. Bath solution contained (in
161 mmol/liter) 140 NaCl, 5.4 KCl, 1.2 KH2PO4, 5 Hepes, 5.55 glucose, 1 MgCl2, 1.8 CaCl2, pH
162 7.4. Once a cell was successfully patched, zero sodium bath solution was introduced into the
163 chamber (mmol/liter) 150 N-methyl-D-glucamine, 2.5 CaCl2, 1 MgCl2, 10 glucose, 10 Hepes,
164 4-amino-pyridine, pH 7.2. Recordings of isoproterenol response were recorded in zero sodium
165 bath solution containing 300 nM isoproterenol. $I_{Ca,L}$ was recorded from a holding potential
166 (V_{hold}) of -50mV. $I_{Ca,T}$ and $I_{Ca,L}$ was recorded from V_{hold} -80mV with 300ms depolarization
167 steps to levels as shown in Figure 4.

168 Calcium transients were recorded from ventricular cardiomyocytes loaded with cell
169 permeable Fura-2-AM (Invitrogen). Cardiomyocytes were field stimulated at 1.0 Hz to
170 determine transient amplitude, upstroke velocity, and rate of decay. All measurements were
171 made following >2 minutes of conditioning of 1 Hz-field stimuli to induce steady state.
172 Transients were recorded at 1 Hz. All Ca^{2+} transient / sarcomere dynamic data were analyzed
173 using IonOptix IonWizard 6.3 (IonOptics Inc., Westwood, MA). Background fluorescence
174 (Fbackground) for F380 and F340 were determined from cell-free regions. Data are expressed
175 as F340/380 and were corrected for Fbackground.

176

177 **Statistics**

178 Values are expressed as mean ± standard error of mean (SEM). We used unpaired
179 Student t test to estimate differences, as appropriate. Throughout the analyses, a P value < 0.05
180 was considered statistically significant. All statistical analyses were performed using the Prism

181 8 software package (GraphPad, La Jolla, CA).

182

Results

Heart structure and coronary tree anatomy are similar between *Acomys* and *Mus*

To establish a basis for accurate comparison across species, we first set out to determine whether baseline differences in cardiac gravimetrics exist between *Acomys* and *Mus*. First, we assessed heart weight (HW) and normalized it to body size (body weight [BW] and tibia length [TL]) to account for overall size differences between species. Although *Acomys* demonstrated a higher mean HW than *Mus* (Figure 1B), normalized to BW, *Acomys* exhibited a slighly lower HW than *Mus* (Figure 1C). There were no differences between species when HW was normalized to TL (Figure 1D). *Acomys* demonstrated heavier wet and dry lung weight than *Mus* (Figure 1E and F), but lower wet and dry lung weight after normalization by BW (Figure 1G and H). However, when normalized by TL, dry and wet lung weight were similar across species (Fig 1I and J). The descriptive analyses are summarized in supplemental table 1.

Next, we compared the gross cardiac structure, coronary tree and vasculature between *Acomys* and *Mus*. Overall, cardiac structure was not visibly different between the species both on gross inspection of the whole heart, short or long axis (Figure 2A) and both species demonstrated similar coronary course with the left anterior descending artery (LAD) supplying the anterior wall and the left circumflex artery supplying the lateral aspect of the left ventricle (Figure 2B-D). Vascular density plays an important role in tissue healing and integrity. Therefore, we assessed vascular density using isolectin staining and observed no significant difference in capillary density between *Mus* and *Acomys* (Figure 2E, F). The descriptive analyses are summarized in supplemental table 1.

Mus and *Acomys* have comparable baseline heart function

Building on our anatomical analyses of *Acomys* and *Mus* hearts, we next performed

208 cardiac echocardiography to compare *in vivo* cardiac function between species. The ejection
209 fraction (EF), fractional shortening (FS), left ventricular end-diastolic diameter (LVEDD), left
210 ventricular end-systolic diameter (LVESD), left ventricular posterior wall thickness (LVPW),
211 and stroke volume were comparable between *Acomys* and *Mus* (Figure 3A-D, F). Left
212 ventricular anterior wall thickness (LVAW) was higher in *Acomys* when compared to *Mus*
213 (Figure 3E). However, when normalized to body weight, LV mass and stroke volume were
214 smaller in *Acomys* (Figure 3G, H). These data support our anatomical data and demonstrate
215 that *in vivo* cardiac function and structure are comparable between species. Furthermore, our
216 functional data provide a baseline for future studies utilizing *Acomys* as a model for cardiac
217 research in comparison to *Mus*. The descriptive analyses are summarized in supplemental table
218 1.
219

220 ***Acomys* cardiomyocytes resemble less mature adult mouse cardiomyocytes**

221 Ventricular cardiomyocyte (CM) phenotype varies across ages and species and plays
222 an important role in cardiac response to injury.[3, 22] During the first week of post-natal life,
223 cardiomyocytes undergo a final burst of DNA replication with and without karyokinesis and
224 therefore most CMs after the first post-natal week are either mononuclear polyploid or
225 multinucleated.[23] In mammals, the presence of mononuclear diploid CMs are indicative of a
226 'young' heart phenotype that is rarely seen in adult mice.[24, 25] To examine CM phenotype
227 between species, we isolated ventricular CMs and stained them with cardiac troponin T (cTnT)
228 and Hoechst. *Acomys* CMs were smaller than *Mus* and were more likely to be mononucleated
229 (Figure 4A-C). *Acomys* CMs also showed reduced t-tubule density and organization compared
230 to *Mus* (Figure 4D-G). We then assessed the ploidy of ventricular CMs across species using
231 flow cytometry as previously described. Our studies demonstrate a significantly higher
232 percentage of diploid CMs in *Acomys* with corresponding lower percentage of tetraploid and

233 >4N CMs (Figure 4H).

234 The relatively small cell size and higher mononucleated percentage in *Acomys* suggest
235 a 'young' cardiomyocyte phenotype. The expression of low-voltage activated (T-type calcium
236 channels) is a hallmark index of relatively immature ventricle; therefore, we recorded voltage-
237 dependent I_{Ca} from *Acomys* ventricular myocytes. From a V_{hold} -80mV, a V_{test} step to -25mV
238 elicits little if any discernable current in *Mus* (Figure 5A, left); by contrast, for V_{test} -25mV
239 *Acomys* cardiomyocytes exhibit a transient 'T-type' calcium current ($I_{Ca,T}$). Longer lasting
240 calcium current ($I_{Ca,L}$) is prominent with larger depolarizations in both *Mus* and *Acomys* (Figure
241 5A, lower panels). The current-voltage relationship shows a prominent $I_{Ca,T}$ component with a
242 peak current between V_{test} -20 and -25mV in *Spiny*, not in *Mus* (Figure 5B).

243 To dissect $I_{Ca,T}$ from $I_{Ca,L}$, we performed current-voltage curve protocols from V_{hold} -
244 50mV to voltage-inactivate the $I_{Ca,T}$ component. Current-voltage relationships for $I_{Ca,T}$-
245 expressing Spiny cells show the prominent $I_{Ca,T}$ appearing as a low-voltage activated current
246 for V_{hold} -80mV but not from V_{hold} – 50 mV (Figure 6A). 33% of *Acomys* ventricular
247 cardiomyocytes show no $I_{Ca,T}$ (Figure 6B) but there was no observed correlation of cell size to
248 presence of ICa,T (Figure 6C). $I_{Ca,T}$ is present in 67% of *Acomys*, compared to <5% of Mus
249 ventricular cardiomyocytes (Figure 6D). Cell capacitance was significantly lower in *Acomys*
250 compared to *Mus* (Figure 6E), consistent with morphometric analysis (above, Figure 4B),.
251 Additionally, maximal conductance density trended greater in *Mus* than *Acomys* (p=0.06,
252 Figure 6F). Voltage-dependent activation and inactivation of $I_{Ca,L}$ was significantly shifted
253 positive for Acomys compared to *Mus* (Figure 6G and H). Taken together these data are
254 consistent with a 'young' adult heart physiological phenotype in the mature *Acomys* heart.

255 We next explored cytosolic calcium handling. Cytosolic Ca^{++} transients (CaT) have a
256 larger amplitude (Figure 7A, 7B), faster upstroke (Figure 7C), and more rapid decay (Figure
257 7D) in *Mus* compared to that in *Acomys*. As with CM morphometrics (Figure 4) and the

prevalent expression of T-type calcium current (Figures 5, 6) the smaller, slower CaT segregate with a less mature CM phenotype. Immature ventricular CM also tend to show reduced β-adrenergic receptor (β-AR) acute responsiveness.[26] Therefore, we tested the effect of isoproterenol challenge (ISO). *Acomys* CaT amplitude remained smaller (Figure 7E, F) and slower (Figure 7G, H). To assess acute responsiveness, we compared within cell before – after ISO. *Mus* shows increased amplitude and more rapid kinetics (Figures 7I-K). By contrast, *Acomys* CaT amplitude and upstroke velocity were not significantly different. Ca^{++} re-uptake was accelerated consistent with only partial β-AR coupling to downstream effectors. Taken together, the *Acomys* ventricular myocardium exhibits a less mature phenotype than *Mus*.

272 **Discussion**

273 The lack of adult mammalian models of cardiac recovery following MI has hampered
274 the field's ability to identify new therapies for heart failure. Based on their enhanced
275 regenerative ability for number of tissue and organs, spiny mice represent a potential model to
276 explore endogenous cardiac repair. In this study, we sought to establish the anatomical and
277 cellular characteristics of *A. cahirinus*, with a specific comparison to the commonly used
278 cardiac murine model, the C57BL6 mouse (*Mus*). Our results demonstrated comparable cardiac
279 structure, anatomy and functional parameters between the two species. Interestingly, we found
280 a significant difference in CM phenotype between species - including smaller cardiomyocyte
281 surface area with less t-tubule density, and more mononucleated, predominantly diploid
282 ventricular cardiomyocytes in mature *Acomys*. Physiological properties reflective of younger
283 cardiomyocytes include expression of $I_{Ca,T}$, lower $I_{Ca,L}$ density and smaller, slower cytosolic
284 CaT. Overall, the outcome of our investigation suggest that *Acomys* may prove to be a useful
285 model for future cardiac regeneration studies.

286 In vertebrate regeneration models, (e.g., axolotl limb, zebrafish heart, *Acomys*
287 musculoskeletal tissue, etc.), tissue is removed by surgical excision and the lost tissue is
288 structurally and functionally replaced.[6, 16, 27] *Acomys* has emerged as a bonafide adult
289 mammalian regeneration model for their ability to regrow complex tissues following full-
290 thickness skin excision[12, 14, 16] and removal of musculoskeletal tissue from the ear pinna.[13, 15,
291 28] In each type of injury, adult *Acomys* were capable of restoring functional, and in some cases,
292 complete scar-free tissues compared to other adult rodents. To establish *Acomys* as an
293 experimental cardiac model, we characterized key anatomical, structural and functional
294 parameters between *Acomys* and the most commonly used experimental *Mus* species (C57Bl/6
295 mice). Our anatomical studies established gross similarity in coronary anatomy between
296 species. *Acomys* and *Mus* have a LAD artery that courses anteriorly below the left atrial

297 appendage, and traverses the anterior interventricular groove supplying the majority of the
298 anterior wall.[29] Similarly, the left coronary artery supplies the lateral and distal anterior wall
299 (Figure 2). Interestingly, *Acomys* hearts were similar structurally and anatomically to *Mus*.
300 Additionally, there were no significant differences for *in vivo* cardiac functional parameters
301 between the two groups (Figure 3). These findings are crucial in planning future myocardial
302 ischemia studies as they indicate that similar techniques can be used to induce comparable
303 injury across species.

304 The adult mammalian heart loses its regenerative capability after the first week of life
305 and heart damage results in permanent loss of myocardium combined with fibrotic scarring and
306 adverse remodeling.[3] The loss of regenerative capability corresponds with loss of CM
307 proliferation as CMs enter cell cycle arrest and become mononuclear polyploid or
308 multinucleated.[3, 30] Therefore, in animal models and humans, cardiac ischemic injury typically
309 leads to the progression of heart failure when the damage is widespread.[9] However, in other
310 vertebrate species where CMs maintain the lifelong ability to proliferate (e.g., zebrafish and
311 newts), cardiac regeneration is still possible.[30, 31] One of the hallmarks of regenerative hearts is
312 the relatively high frequency of mononucleated diploid CMs. Indeed, both neonatal mice and
313 adult zebrafish with high percentage of mononuclear diploid CMs can regenerate cardiac tissue
314 after injury via the proliferation of pre-existing CMs.[32] Taken together, this data suggests that
315 higher proportions of mononuclear diploid CMs are associated with higher regenerative
316 capacity. A recent study further reported that the proportion of mononuclear cardiomyocytes
317 varied more than 7-fold in 120 inbred adult mouse strains, and a higher proportion of
318 mononuclear cardiomyocytes was associated with improved EF after myocardial infarction.[22]
319 Our study examined the nucleation and ploidy of *Acomys* and *Mus* and established that *Acomys*
320 have a higher proportion of mononucleated and diploid cardiomyocytes that are smaller in size
321 resembling those of neonatal mice (Figure 4A-C, H). Future studies are planned to examine the

322 proliferative potential of CMs in *Acomys* and *Mus* and their potential to adequately respond to
323 myocardial injury.

324 There are two types of Ca^{++} channels in cardiomyocytes, L-type and T-type. L-type
325 Ca^{++} channels are highly expressed in the adult heart and are important therapeutic targets for
326 the management of various cardiovascular diseases. In contrast to L-type channels, T-type Ca^{++}
327 channels are rarely found in adults and are present in the hearts of fetal and early postnatal mice
328 that have the ability to regenerate cardiomyocytes.[33] In our cell electrophysiology studies,
329 *Acomys* exhibit T-type Ca^{++} channels (Figure 6A-D). This feature is consistent with *Acomys*
330 cardiomyocytes exhibiting a 'younger' phenotype compared to *Mus*. Furthermore, immature
331 ventricular cardiomyocytes show reduced Ca^{++} transient amplitude, slower kinetics,[34] and
332 attenuated β-adrenergic receptor responsiveness.[35] In concert with the reduced t-tubule density
333 the overall picture emerges that the adult *Acomys* ventricular cardiomyocytes retain a more
334 'youthful' phenotype.

335 In conclusion, spiny mice represent a novel model for cardiac research. *Acomys*
336 demonstrate comparable cardiac structure, function and anatomy when compared to *Mus*,
337 aiding in ease of interpretation of future experimental results. However, ventricular CM
338 phenotype in *Acomys* represent a significant departure from those seen in adult *Mus* with
339 distinct features such as smaller surface area, abundance of T-type calcium currents and a
340 higher percentage of mononucleated and diploid cells; phenotypic differences that are typical
341 of species capable of cardiac regeneration. Future studies will focus on the potential of these
342 phenotypic differences to foster regeneration and repair instead of scarring and heart failure in
343 models of cardiac disease.
344
345

346 **References.**

347 1. Benjamin EJ, Blaha MJ, Chiuve SE, Cushman M, Das SR, Deo R, de Ferranti SD, Floyd J,
348 Fornage M, Gillespie C, Isasi CR, Jimenez MC, Jordan LC, Judd SE, Lackland D, Lichtman JH,
349 Lisabeth L, Liu S, Longenecker CT, Mackey RH, Matsushita K, Mozaffarian D, Mussolino ME,
350 Nasir K, Neumar RW, Palaniappan L, Pandey DK, Thiagarajan RR, Reeves MJ, Ritchey M,
351 Rodriguez CJ, Roth GA, Rosamond WD, Sasson C, Towfighi A, Tsao CW, Turner MB, Virani
352 SS, Voeks JH, Willey JZ, Wilkins JT, Wu JH, Alger HM, Wong SS, Muntner P, American Heart
353 Association Statistics C, Stroke Statistics S. Heart disease and stroke statistics-2017 update: A
354 report from the american heart association. *Circulation*. 2017;135:e146-e603
355 2. McAloon CJ, Boylan LM, Hamborg T, Stallard N, Osman F, Lim PB, Hayat SA. The changing
356 face of cardiovascular disease 2000-2012: An analysis of the world health organisation global
357 health estimates data. *Int J Cardiol*. 2016;224:256-264
358 3. Porrello ER, Mahmoud AI, Simpson E, Hill JA, Richardson JA, Olson EN, Sadek HA. Transient
359 regenerative potential of the neonatal mouse heart. *Science*. 2011;331:1078-1080
360 4. Bader D, Oberpriller JO. Repair and reorganization of minced cardiac muscle in the adult newt
361 (notophthalmus viridescens). *J Morphol*. 1978;155:349-357
362 5. Flink IL. Cell cycle reentry of ventricular and atrial cardiomyocytes and cells within the
363 epicardium following amputation of the ventricular apex in the axolotl, amblystoma mexicanum:
364 Confocal microscopic immunofluorescent image analysis of bromodeoxyuridine-labeled nuclei.
365 *Anat Embryol (Berl)*. 2002;205:235-244
366 6. Poss KD, Wilson LG, Keating MT. Heart regeneration in zebrafish. *Science*. 2002;298:2188-
367 2190
368 7. Pfeffer MA, Braunwald E. Ventricular remodeling after myocardial infarction. Experimental
369 observations and clinical implications. *Circulation*. 1990;81:1161-1172
370 8. Jugdutt BI. Ventricular remodeling after infarction and the extracellular collagen matrix: When
371 is enough enough? *Circulation*. 2003;108:1395-1403
372 9. Struthers AD. Pathophysiology of heart failure following myocardial infarction. *Heart*. 2005;91
373 Suppl 2:ii14-16; discussion ii31, ii43-18
374 10. Honkoop H, de Bakker DE, Aharonov A, Kruse F, Shakked A, Nguyen PD, de Heus C, Garric
375 L, Muraro MJ, Shoffner A, Tessadori F, Peterson JC, Noort W, Bertozzi A, Weidinger G,
376 Posthuma G, Grun D, van der Laarse WJ, Klumperman J, Jaspers RT, Poss KD, van
377 Oudenaarden A, Tzahor E, Bakkers J. Single-cell analysis uncovers that metabolic
378 reprogramming by erbb2 signaling is essential for cardiomyocyte proliferation in the
379 regenerating heart. *Elife*. 2019;8
380 11. Haughton CL, Gawriluk TR, Seifert AW. The biology and husbandry of the african spiny mouse
381 (acomys cahirinus) and the research uses of a laboratory colony. *J Am Assoc Lab Anim Sci*.
382 2016;55:9-17
383 12. Brant JO, Yoon JH, Polvadore T, Barbazuk WB, Maden M. Cellular events during scar-free skin

regeneration in the spiny mouse, acomys. *Wound Repair Regen*. 2016;24:75-88

13. Gawriluk TR, Simkin J, Thompson KL, Biswas SK, Clare-Salzler Z, Kimani JM, Kiama SG, Smith JJ, Ezenwa VO, Seifert AW. Comparative analysis of ear-hole closure identifies epimorphic regeneration as a discrete trait in mammals. *Nat Commun*. 2016;7:11164

14. Jiang TX, Harn HI, Ou KL, Lei M, Chuong CM. Comparative regenerative biology of spiny (acomys cahirinus) and laboratory (mus musculus) mouse skin. *Exp Dermatol*. 2019;28:442-449

15. Matias Santos D, Rita AM, Casanellas I, Brito Ova A, Araujo IM, Power D, Tiscornia G. Ear wound regeneration in the african spiny mouse acomys cahirinus. *Regeneration (Oxf)*. 2016;3:52-61

16. Seifert AW, Kiama SG, Seifert MG, Goheen JR, Palmer TM, Maden M. Skin shedding and tissue regeneration in african spiny mice (acomys). *Nature*. 2012;489:561-565

17. Okamura DM, Brewer CM, Wakenight P, Bahrami N, Bernardi K, Tran A, Olson J, Shi X, Piliponsky AM, Nelson BR, Beier DR, Millen KJ, Majesky MW. Scarless repair of acute and chronic kidney injury in african spiny mice (acomys cahirinus). *bioRxiv*. 2018;315069.

18. Al-Darraji A, Haydar D, Chelvarajan L, Tripathi H, Levitan B, Gao E, Venditto VJ, Gensel JC, Feola DJ, Abdel-Latif A. Azithromycin therapy reduces cardiac inflammation and mitigates adverse cardiac remodeling after myocardial infarction: Potential therapeutic targets in ischemic heart disease. *PLoS One*. 2018;13:e0200474

19. Ahern BM, Levitan BM, Veeranki S, Shah M, Ali N, Sebastian A, Su W, Gong MC, Li J, Stelzer JE, Andres DA, Satin J. Myocardial-restricted ablation of the gtpase rad results in a pro-adaptive heart response in mice. *J Biol Chem*. 2019;294:10913-10927

20. Guo A, Song LS. Autott: Automated detection and analysis of t-tubule architecture in cardiomyocytes. *Biophys J*. 2014;106:2729-2736

21. Windmueller R, Leach JP, Babu A, Zhou S, Morley MP, Wakabayashi A, Petrenko NB, Viatour P, Morrisey EE. Direct comparison of mononucleated and binucleated cardiomyocytes reveals molecular mechanisms underlying distinct proliferative competencies. *Cell Rep*. 2020;30:3105-3116 e3104

22. Patterson M, Barske L, Van Handel B, Rau CD, Gan P, Sharma A, Parikh S, Denholtz M, Huang Y, Yamaguchi Y, Shen H, Allayee H, Crump JG, Force TI, Lien CL, Makita T, Lusis AJ, Kumar SR, Sucov HM. Frequency of mononuclear diploid cardiomyocytes underlies natural variation in heart regeneration. *Nat Genet*. 2017;49:1346-1353

23. Shen H, Gan P, Wang K, Darehzereshki A, Wang K, Kumar SR, Lien CL, Patterson M, Tao G, Sucov HM. Mononuclear diploid cardiomyocytes support neonatal mouse heart regeneration in response to paracrine igf2 signaling. *Elife*. 2020;9

24. Alkass K, Panula J, Westman M, Wu TD, Guerquin-Kern JL, Bergmann O. No evidence for cardiomyocyte number expansion in preadolescent mice. *Cell*. 2015;163:1026-1036

25. Soonpaa MH, Kim KK, Pajak L, Franklin M, Field LJ. Cardiomyocyte DNA synthesis and

422 binucleation during murine development. *Am J Physiol*. 1996;271:H2183-2189
423 26. Schroder E, Byse M, Satin J. L-type calcium channel c terminus autoregulates transcription. *Circ*
424 *Res*. 2009;104:1373-1381
425 27. Haas BJ, Whited JL. Advances in decoding axolotl limb regeneration. *Trends Genet*.
426 2017;33:553-565
427 28. Simkin J, Gawriluk TR, Gensel JC, Seifert AW. Macrophages are necessary for epimorphic
428 regeneration in african spiny mice. *Elife*. 2017;6
429 29. Ostadal B, Schiebler TH, Rychter Z. Relations between development of the capillary wall and
430 myoarchitecture of the rat heart. *Adv Exp Med Biol*. 1975;53:375-388
431 30. Kikuchi K, Holdway JE, Werdich AA, Anderson RM, Fang Y, Egnaczyk GF, Evans T, Macrae CA,
432 Stainier DY, Poss KD. Primary contribution to zebrafish heart regeneration by gata4(+)
433 cardiomyocytes. *Nature*. 2010;464:601-605
434 31. Oberpriller JO, Oberpriller JC. Response of the adult newt ventricle to injury. *J Exp Zool*.
435 1974;187:249-253
436 32. Jopling C, Sleep E, Raya M, Marti M, Raya A, Izpisua Belmonte JC. Zebrafish heart regeneration
437 occurs by cardiomyocyte dedifferentiation and proliferation. *Nature*. 2010;464:606-609
438 33. Cribbs LL, Martin BL, Schroder EA, Keller BB, Delisle BP, Satin J. Identification of the t-type
439 calcium channel (ca(v)3.1d) in developing mouse heart. *Circ Res*. 2001;88:403-407
440 34. Balaguru D, Haddock PS, Puglisi JL, Bers DM, Coetzee WA, Artman M. Role of the
441 sarcoplasmic reticulum in contraction and relaxation of immature rabbit ventricular myocytes. *J*
442 *Mol Cell Cardiol*. 1997;29:2747-2757
443 35. Kuznetsov V, Pak E, Robinson RB, Steinberg SF. Beta 2-adrenergic receptor actions in neonatal
444 and adult rat ventricular myocytes. *Circ Res*. 1995;76:40-52

445

446

447 **Figure legend.**

448

449 **Figure 1. *Acomys* heart is heavier than *Mus*, but heart size is no significant different.**

450 (A) The quantitation of body weight (BW) of *Mus* (n = 10) and *Acomys* (n = 22). (B, C, D) The
451 quantitation of heart weight (HW) of *Mus* (n = 10) and *Acomys* (n = 23), HW normalized by
452 BW of *Mus* (n = 10) and *Acomys* (n = 23), and HW normalized by tibial length (TL) of *Mus* (n
453 = 6) and *Acomys* (n = 17). Values are means ± S.E.M. *P < 0.05 compared to *Mus*. (E-J) The
454 quantitation of wet and dry lung weight (LW) of *Mus* (n = 10) and *Acomys* (n = 20) , wet and
455 dry LW normalized by BW of *Mus* (n = 10) and *Acomys* (n = 20), and wet and dry LW
456 normalized by TL of *Mus* (n = 6) and *Acomys* (n = 17) (Values are means ± S.E.M, *P < 0.05
457 compared to *Mus*).

458

459 **Figure 2. Coronary anatomy in *Mus* and *Acomys*.**

460 (A) Representative whole hearts of *Mus* (left) and *Acomys* (right) at baseline. (B) A schematic
461 of the coronary anatomy in mice. **Panel C** shows representative images of the blood supply of
462 the anterior and posterior wall across species using TRITC-Dextran IV infusion prior to
463 sacrifice. Hearts were imaged using the Maestro EX system (red arrows are left anterior
464 descending artery). The lower panel shows the coronary anatomy of the posterior wall. **Panel**
465 **D** demonstrates the left anterior descending artery across species using intra-aortic infusion of
466 Batson's 17 polymer mixture (Scale bar represents 1 mm). (E) Representative isolectin staining
467 (Red) for capillary density at baseline. Scale bar represents 50 μm. (F) Quantitative analysis of
468 capillary density for *Mus* and *Acomys*. n = 4 mice for each group (Values are means ± S.E.M).

469

470 **Figure 3. Cardiac function by echocardiograph at baseline.**

471 M-mode echocardiography of *Mus* (left) and *Acomys* (right) at baseline (top images). Ejection
472 fraction (A), fractional shortening (B), left ventricular end-diastolic diameter (LVEDD) (C),
473 left ventricular end-systolic diameter (LVESD) (D), left ventricular anterior wall (LVAW) (E),

474 left ventricular posterior wall (LVPW) (F), LV mass normalized by body weight (BW) (G), and
475 stroke volume normalized by BW (H) were comparable when measured by echocardiography
476 in *Mus* and *Acomys* at baseline (n = 30 *Mus* and 10 *Acomys*) (Values are means ± S.E.M, *$P <$
477 0.05 compared to *Mus*).
478
479 **Figure 4. Characteristics of cardiomyocyte in *Acomys* resemble neonatal mouse**
480 **cardiomyocytes.**
481 (A) Single-cell ventricular suspension stained with cardiac troponin T (cTnT) (red) and with
482 Hoechst (blue), identifying a small mononuclear cardiomyocyte on *Acomys*, and to a larger
483 binucleated cardiomyocyte on *Mus*. Scale bar represents 50 μm. (B) The quantitation of cell
484 surface area of cardiomyocytes. This graph shows the cell surface area of *Mus* and *Acomys*. All
485 cells (n = 100, each animal) randomly selected (n = 6 mice for *Mus* and 4 mice for *Acomys*, *P
486 < 0.05 compared to *Mus*. Values are means ± S.E.M). (C) Calculation of percentage of
487 mononuclear cardiomyocytes for *Mus* and *Acomys* (n = 4 mice for each group, values are means
488 ± S.E.M, *P < 0.05 compared to *Mus*). (D, E, F, G) Single cell pooled t-tubule analysis shows
489 significantly greater t-tubule density in transverse (E) and axial directions (F) along with wider
490 t-tubule spacing (G) in *Acomys* compared to *Mus* (****p<0.001, scale bar = 50 μm). (H)
491 Calculation of percentage of ploidy in cardiomyocytes for *Mus* and *Acomys* by Flow cytometry
492 (n = 2 mice/group, values are means ± S.E.M).
493
494 **Figure 5. Calcium current in *Acomys* and *Mus.***
495 (A) Current traces elicited by V_{test} -25 mV (upper) & V_{test} +15mV (lower) from V_{hold} -80 mV.
496 (B) Current-voltage relationships shows evidence for $I_{Ca,T}$ in *Acomys*, but not in *Mus*. For
497 *Acomys*, n=9 cells; N=5 animals; for *Mus*, n=44, N=13 animals.
498

499 **Figure 6. $I_{Ca,T}$ measurements indicating less mature ventricular cardiomyocytes in**
500 ***Acomys*.**
501 (A, B) Current-voltage curves from V_{hold} -80mV and -50 mV superimposed for *Acomys* CM
502 exhibiting $I_{Ca,T}$ (A) or no $I_{Ca,T}$ (B). (C) Cell capacitance was not different for *Acomys* CM with
503 or without $I_{Ca,T}$. (D) $I_{Ca,T}$ expression was heterogeneous but more *Acomys* ventricular CMs
504 showed $I_{Ca,T}$ compared to rare occurrences in *Mus*. (E) Cell capacitance was greater in *Mus*
505 than *Acomys*. $^{**}P<0.01$. (F) Maximal conductance density trended greater in *Mus* than *Acomys*.
506 $P=0.06$. G) Voltage-dependent activation and inactivation (H) of $I_{Ca,L}$ was significantly shifted
507 positive for *Acomys* compared to *Mus* ($^{****}P<0.001$).
508
509 **Figure 7. Calcium transients in *Mus* and *Acomys*.**
510 (A) Representative calcium transients from isolated ventricular cardiomyocytes loaded with
511 fura2-AM, *Mus* (top, red) and *Acomys* (bottom, blue) paced at 1 Hz. Scale bar: 2 seconds. (B)
512 Amplitude of the transients ($^{***}P = 0.0004$). (C) Velocity at which calcium enters the cytosol
513 (upstroke of the transient: $^{*}P=0.04$). (D) Calcium transient decay ($^{***}P=0.0005$). (E)
514 Representative calcium transients treated with 100 nM isoproterenol (ISO), *Mus* (top, red) and
515 *Acomys* (bottom, blue), paced at 1 Hz. Scale bar: 2 seconds. (F) Amplitude of the transients
516 with ISO ($^{*}P= 0.04$). (G) Velocity at which calcium enters the cytosol with ISO ($^{*}P= 0.05$).
517 (H) Calcium transient decay with ISO ($^{****}P<0.0001$). (I) Before and after ISO Amplitude of
518 the transients ($^{**}P= 0.007$). (J) Before and after ISO Velocity at which calcium enters the
519 cytosol ($P = 0.02$). (K) Calcium transient decay ($^{***}P = 0.002$). N = 7 animals and 37 cells for
520 *Mus*; and 4 animals and 31 cells for *Acomys*.
521
522
523
524

525 **Supplemental table 1.**

		Mus			*Acomys*			
		n	Mean	SEM	n	Mean	SEM	*P-value*
Structural parameters								
	BW (mg)	10	26.92	1.12	22	50.26	2.18	<0.0001*
	HW (mg)	10	167.58	10.41	23	231.07	12.92	0.0034*
	HW / BW	10	6.22	0.29	23	4.59	0.34	0.0058*
	HW / TL	6	96.60	8.31	17	95.81	5.59	0.8648
	Wet LW (mg)	10	161.40	12.55	20	204.03	9.92	0.0222*
	Dry LW (mg)	10	34.91	2.42	20	41.83	2.71	0.0479*
	Wet LW / BW	10	5.98	0.36	20	4.00	0.20	<0.0001*
	Dry LW / BW	10	1.30	0.07	20	0.81	0.05	<0.0001*
	Wet LW / TL	6	80.62	5.99	17	92.72	5.45	0.2273
	Dry LW / TL	6	18.19	1.15	17	18.38	1.39	0.6088
Cardiac function								
	EF (%)	30	62.94	0.94	10	65.93	1.89	0.1314
	% FS	30	33.63	0.67	10	35.01	1.35	0.3626
	LVEDD (mm)	30	3.72	0.04	10	3.79	0.11	0.3964
	LVESD (mm)	30	2.46	0.04	10	2.47	0.10	0.7179
	LVAW (mm)	30	0.78	0.02	10	0.88	0.02	0.0014*
	LVPW (mm)	30	0.8210	0.0164	10	0.8951	0.0351	0.0707
	LV mass / BW	30	3.31	0.07	10	2.42	0.10	<0.0001*

	Stroke volume / BW	27	1.59	0.03	7	0.95	0.06	<0.0001*
Cardiomyocyte characteristic								
	Cell surface area (μm^2)	6	2719.18	193.29	4	699.69	48.01	0.0095*
	% mononuclear	4	6.32	1.89	4	16.90	0.82	0.0061*
	Vessel density ($/mm^2$)	4	2736.29	209.44	4	2431.86	249.80	0.6857

BW; body weight, HW; heart weight, TL; tibial length, LW; lung wight, EF; ejection fraction, LVEDD; left ventricular end-diastolic diameter, LVESD; left ventricular end-systolic diameter, LVAW; left ventricular anterior wall, LV mass; left ventricular mass (*$P < 0.05$).

Figure 1

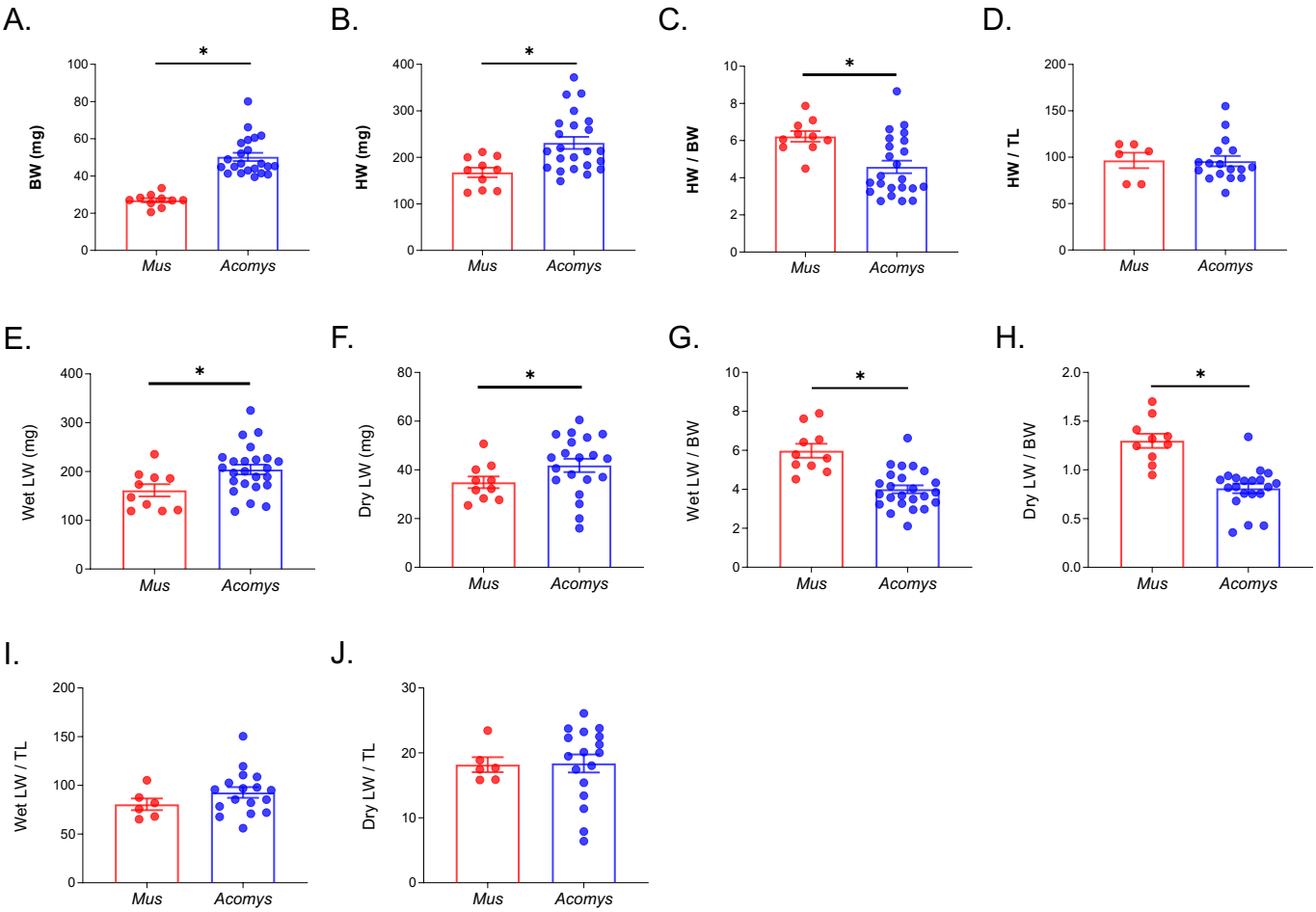
A.
BW (mg)
100
80
60
40
20
0
*
Mus
Acomys
B.
HW (mg)
400
300
200
100
0
*
Mus
Acomys
C.
HW / BW
10
8
6
4
2
0
*
Mus
Acomys
D.
HW / TL
200
150
100
50
0
Mus
Acomys
E.
Wet LW (mg)
400
300
200
100
0
*
Mus
Acomys
F.
Dry LW (mg)
80
60
40
20
0
*
Mus
Acomys
G.
Wet LW / BW
10
8
6
4
2
0
*
Mus
Acomys
H.
Dry LW / BW
2.0
1.5
1.0
0.5
0.0
*
Mus
Acomys
I.
Wet LW / TL
200
150
100
50
0
Mus
Acomys
J.
Dry LW / TL
30
20
10
0
Mus
Acomys

Figure 2

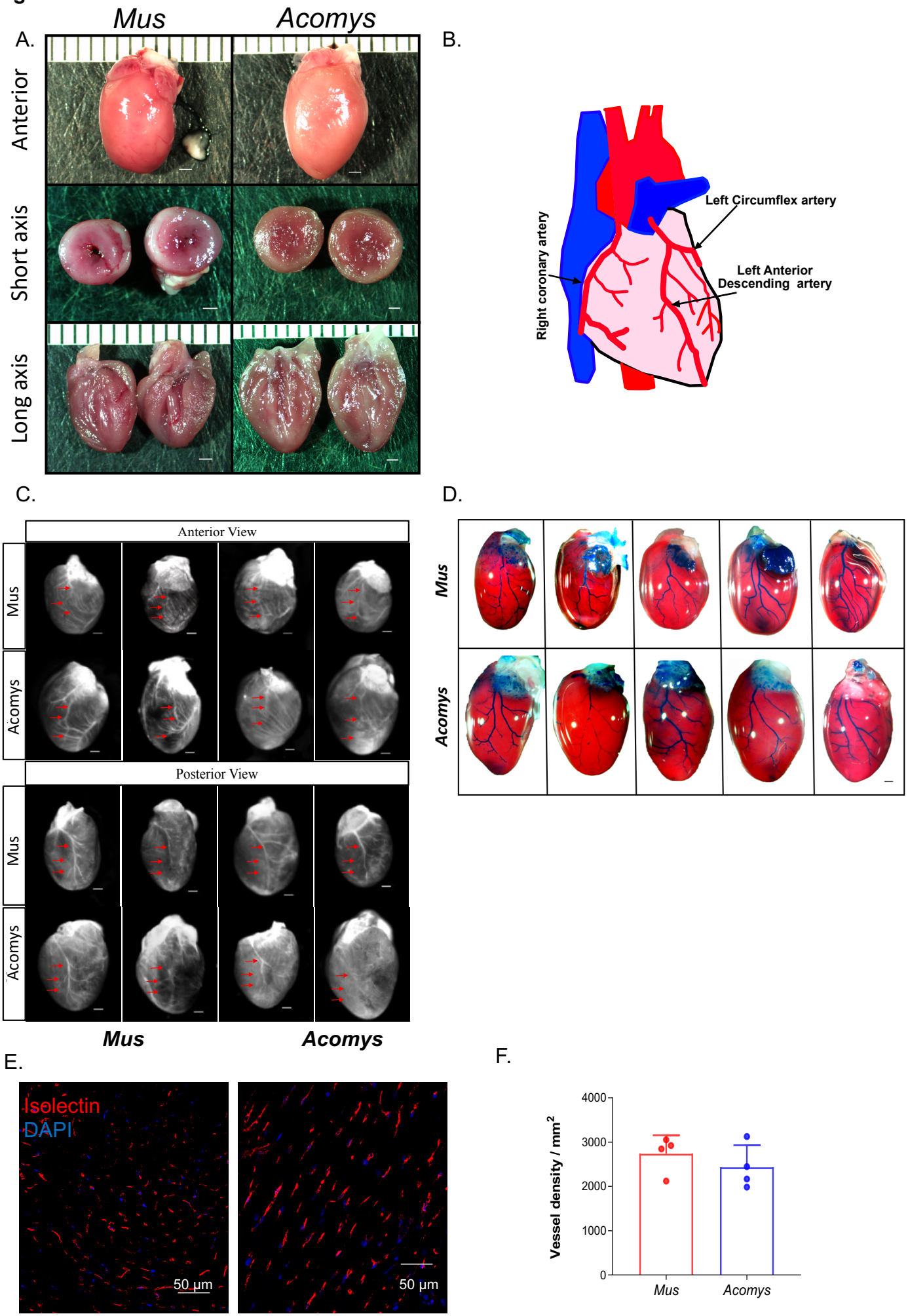
A.
Mus
Acomys
Anterior
Short axis
Long axis
B.
Left Circumflex artery
Left Anterior Descending artery
Right coronary artery
C.
Anterior View
Mus
Acomys
Posterior View
Mus
Acomys
Mus
Acomys
D.
Mus
Acomys
E.
Isolectin
DAPI
50 µm
50 µm
F.
Vessel density / mm²
4000
3000
2000
1000
0
Mus
Acomys

Figure 3

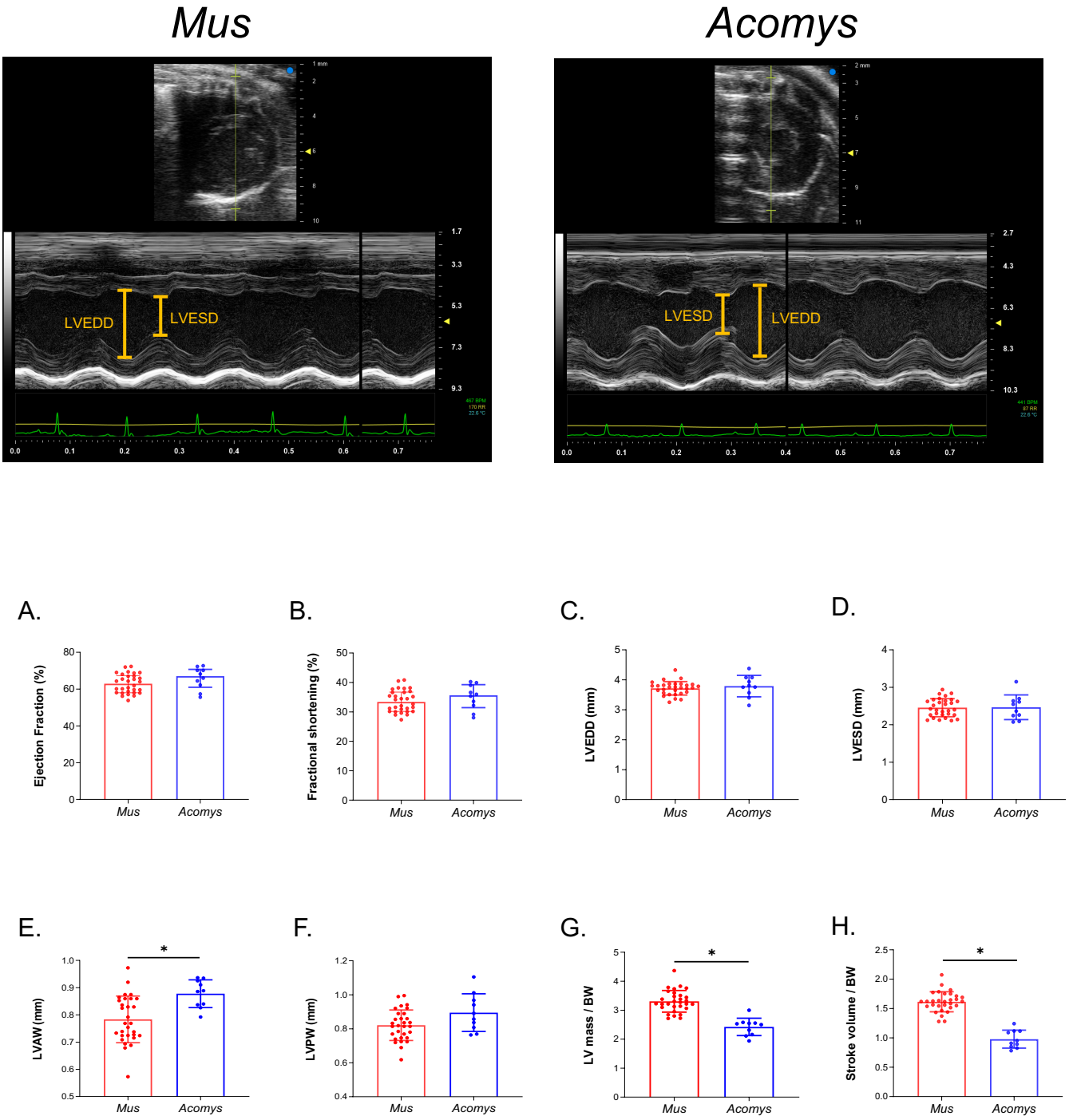
Mus
Acomys
LVEDD
LVESD
LVESD
LVEDD
A.
Ejection Fraction (%)
B.
Fractional shortening (%)
C.
LVEDD (mm)
D.
LVESD (mm)
E.
LVAW (mm)
F.
LVPW (mm)
G.
LV mass / BW
H.
Stroke volume / BW
Mus
Acomys
*

Figure 4

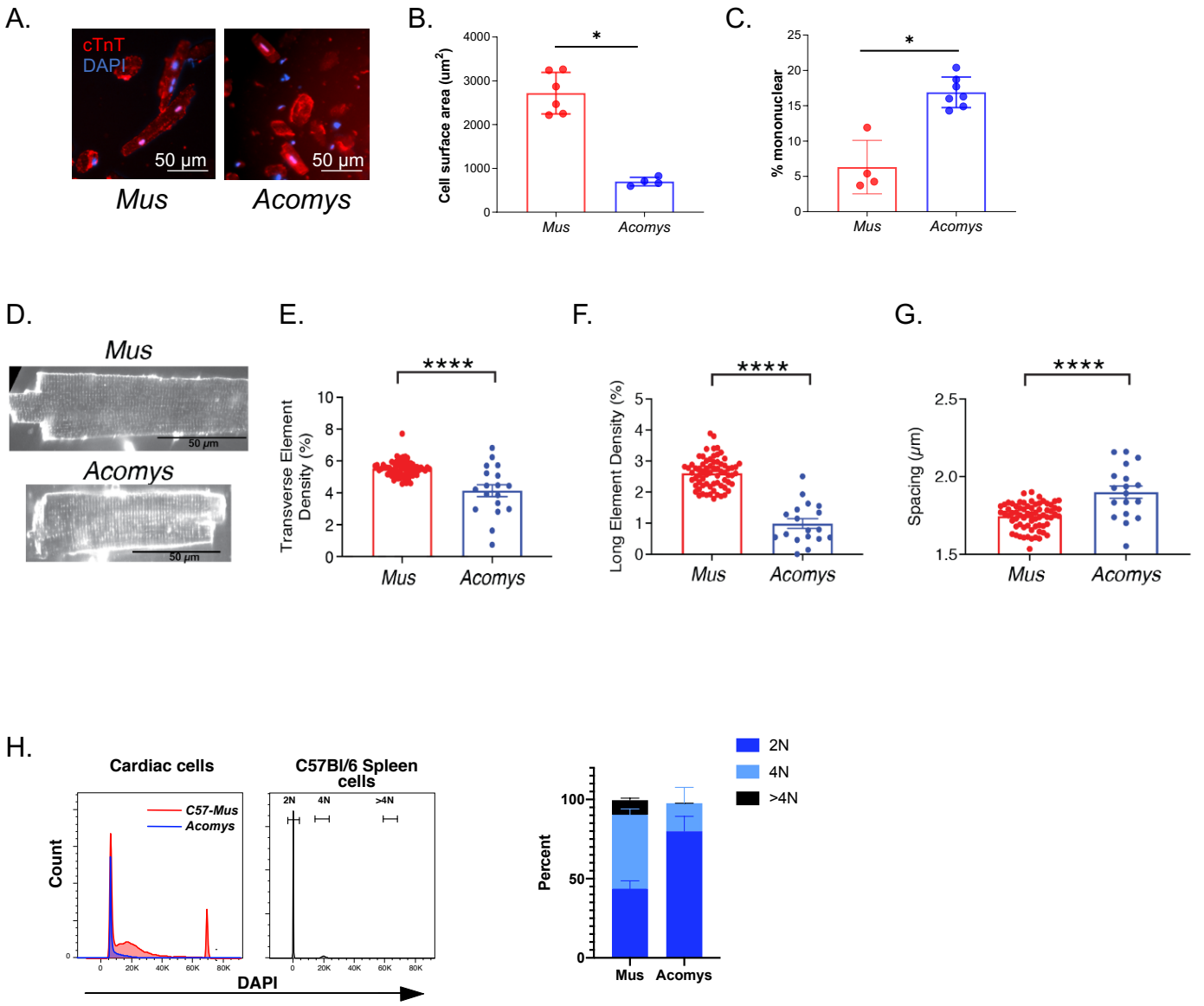
A.
cTnT
DAPI
50 µm
50 µm
Mus
Acomys
B.
Cell surface area (um²)
4000
3000
2000
1000
0
*
Mus
Acomys
C.
% mononuclear
25
20
15
10
5
0
*
Mus
Acomys
D.
Mus
50 µm
Acomys
50 µm
E.
Transverse Element Density (%)
10
8
6
4
2
0
****
Mus
Acomys
F.
Long Element Density (%)
5
4
3
2
1
0
****
Mus
Acomys
G.
Spacing (µm)
2.5
2.0
1.5
****
Mus
Acomys
H.
Cardiac cells
C57Bl/6 Spleen cells
C57-Mus
Acomys
Count
2N
4N
>4N
0
20K
40K
60K
80K
DAPI
2N
4N
>4N
Percent
100
50
0
Mus
Acomys

Figure 5

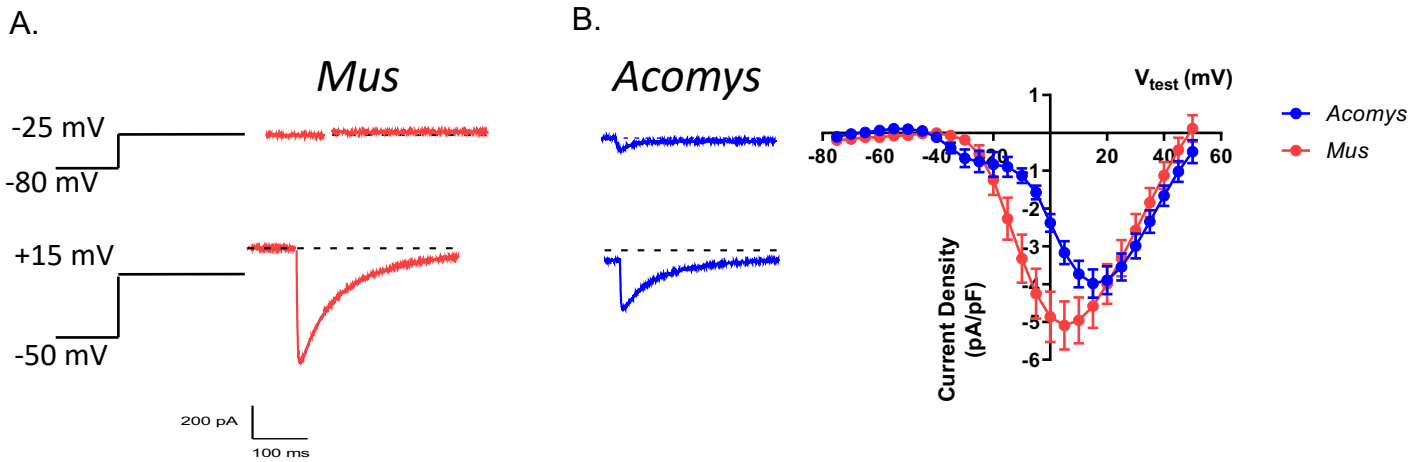
A.
Mus
-25 mV
-80 mV
+15 mV
-50 mV
200 pA
100 ms
B.
Acomys
Vtest (mV)
Current Density (pA/pF)
Acomys
Mus

Figure 6

A.

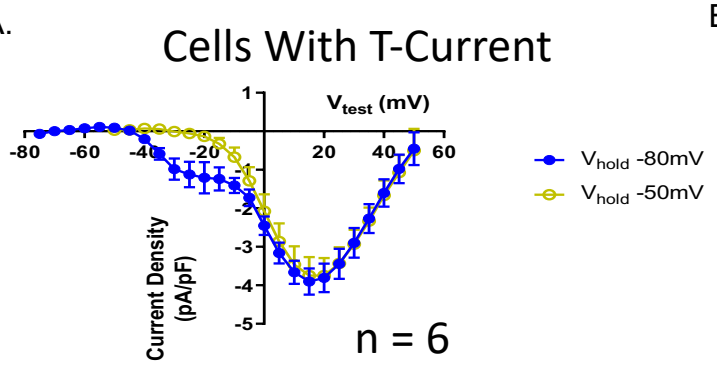

B.

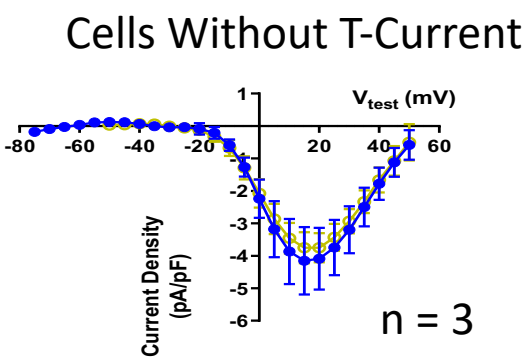

C.

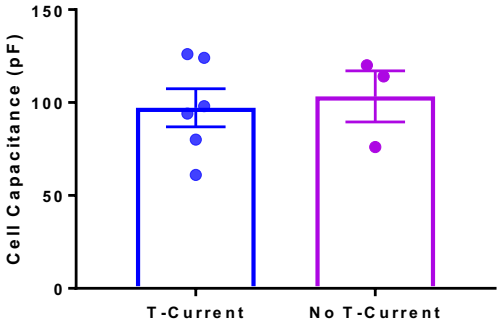

D.

Prevalence of $I_{Ca,T}$

	Mus	*Acomys*
Total cells	44	9
$I_{Ca,T}$ Positive	2	6
Fraction of cells with $I_{Ca,T}$	<5%	67%***

***$p<10^{-3}$; Fisher's exact test

E.

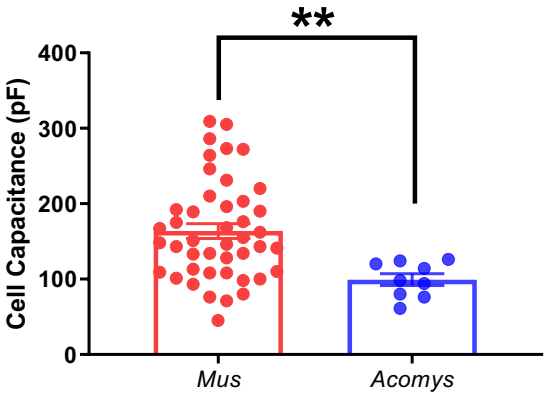

F.

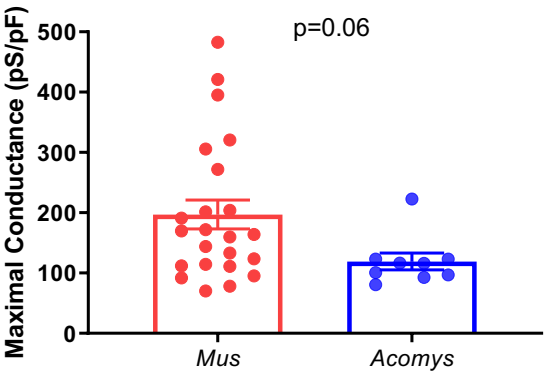

G.

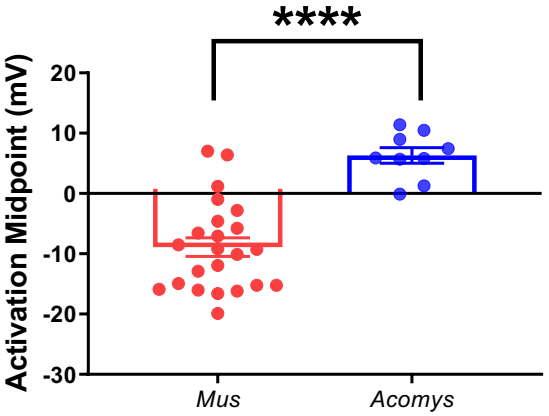

H.

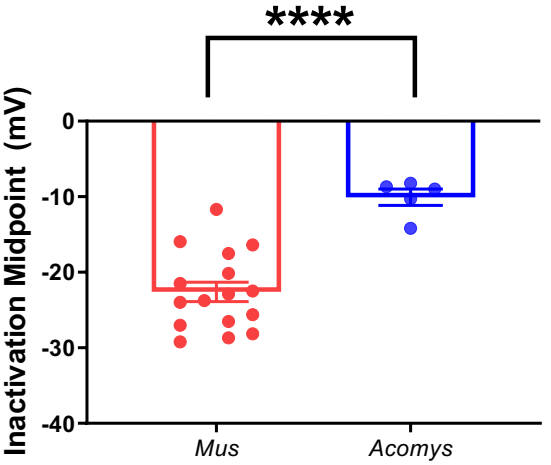

Figure 7

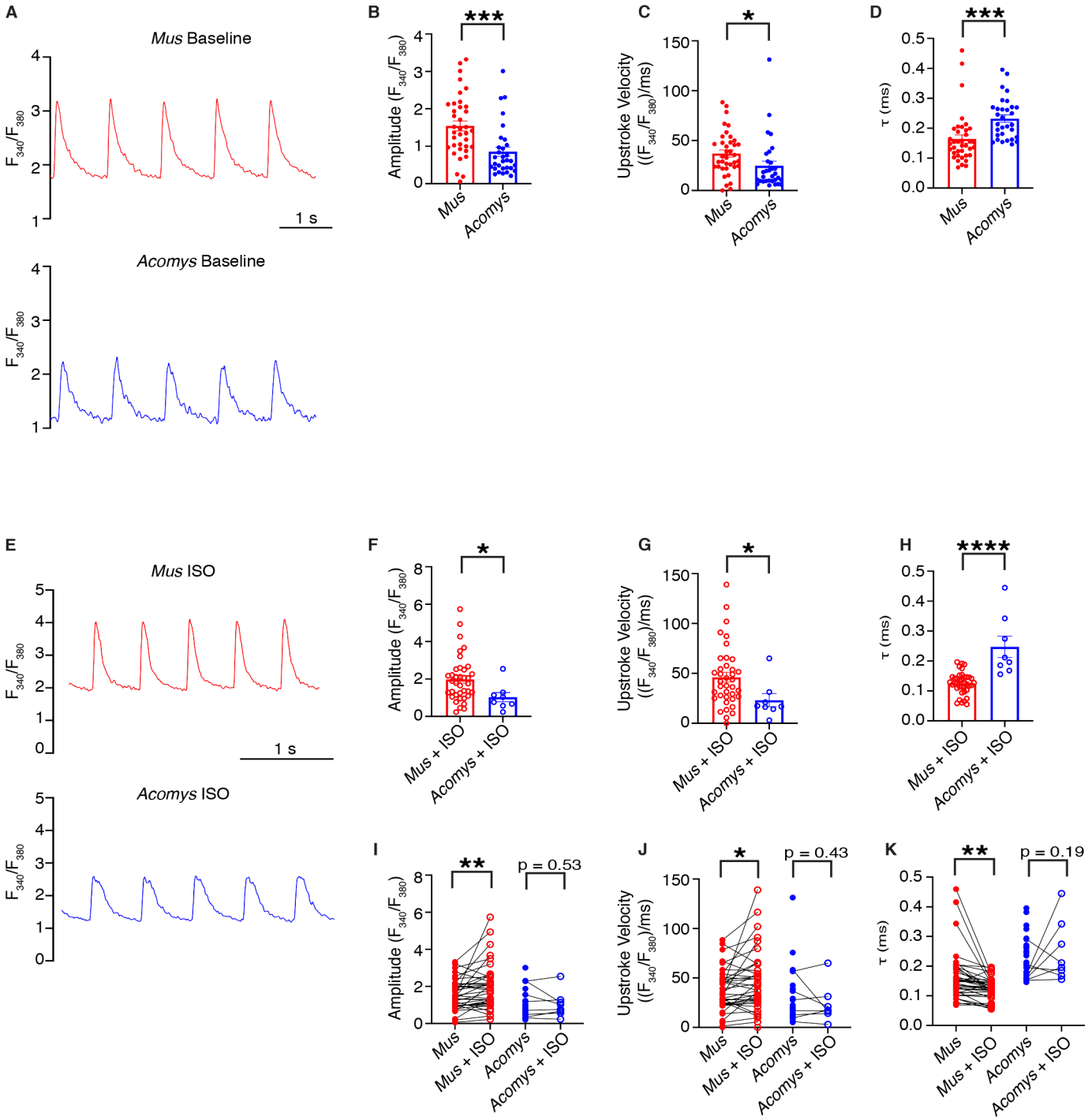
A
Mus Baseline
Acomys Baseline
F340/F380
1 s
B
Amplitude (F340/F380)
***
Mus
Acomys
C
Upstroke Velocity ((F340/F380)/ms)
*
D
τ (ms)
***
E
Mus ISO
Acomys ISO
F
Mus + ISO
Acomys + ISO
G
H
****
I
**
p = 0.53
J
p = 0.43
K
p = 0.19